Article

Tuning the Structural and Physical Properties of CrTiSe by Lithium Intercalation: A Study of the Magnetic Properties, Investigation of Ion Mobility with NMR Spectroscopy and Electronic Band Structure Calculations

Joseph Wontcheu, Wolfgang Bensch, Martin Wilkening, Paul Heitjans, Sylvio Indris, Paul Sideris, Clare P. Grey, Sergiy Mankovsky, and Hubert Ebert

J. Am. Chem. Soc., **2008**, 130 (1), 288-299 • DOI: 10.1021/ja076082+

J|A|C|S
ARTICLES
Published on Web 12/13/2007

Tuning the Structural and Physical Properties of $Cr_2Ti_3Se_8$ by Lithium Intercalation: A Study of the Magnetic Properties, Investigation of Ion Mobility with NMR Spectroscopy and Electronic Band Structure Calculations

Joseph Wontcheu,[†] Wolfgang Bensch,*[,†] Martin Wilkening,[‡] Paul Heitjans,[‡] Sylvio Indris,[§] Paul Sideris,[§] Clare P. Grey,[§] Sergiy Mankovsky,[||] and Hubert Ebert[||]

Institute of Inorganic Chemistry, University of Kiel, Olshausenstrasse 40-60, D-24098 Kiel, Germany, Institute of Physical Chemistry and Electrochemistry, Leibniz University Hannover, and Center for Solid State Chemistry and New Materials (ZFM), Leibniz University Hannover, Callinstrasse 3-3a, D-30167 Hannover, Germany, Chemistry Department, State University of New York at Stony Brook, 100 Nichols Road, Stony Brook, New York 11794-3400, and Department of Chemistry and Biochemistry, LMU-Munich, Butenandtstr. 5-13, D-81377 Munich, Germany

Received August 16, 2007; E-mail: wbensch@ac.uni-kiel.de

Abstract: The room temperature intercalation of $Cr_2Ti_3Se_8$ with butyl lithium yields a phase mixture of the starting material and of the new trigonal phase with composition $Li_{0.4}Cr_{0.5}Ti_{0.75}Se_2$. The phase pure fully intercalated trigonal phase is obtained at elevated temperature (80 °C) with the final composition $Li_{0.62}Cr_{0.5}Ti_{0.75}Se_2$. The line profile analysis (LPA) of the powder patterns shows that pronounced strain occurs in the intercalated material. The deintercalation of the material is realized by treatment of the fully intercalated sample with distilled water leading to the composition $Li_{0.15}Cr_{0.5}Ti_{0.75}Se_2$. The intercalation is accompanied by an electron transfer from the guest Li to the host material, and as a consequence significant changes of the interatomic distances are observed. The local environment and the dynamics of the Li^+ ions in the fully intercalated sample were studied with ^7Li magic angle spinning (MAS) NMR investigations. These reveal different environments of transition metal neighbors for the Li sites and a high mobility of the Li ions. Magnetic measurements show that in the pristine material antiferromagnetic interactions are dominating ($\theta = -113.5$ K) with no long-range order at low temperatures. The magnetic ground state is characterized by a spin-glass behavior. With increasing Li content the antiferromagnetic character vanishes progressively, and the fully intercalated phase exhibits a positive Weiss constant ($\theta = 12$ K) indicating dominating ferromagnetic exchange interactions; i.e., the magnetic properties can be significantly altered by lithiation. The interpretation of our experimental findings is supported by the results of accompanying band structure calculations done within the framework of local spin density functional theory. These demonstrate in particular the role of the charge transfer between the constituents as a function of the Li concentration and its impact on the exchange coupling.

Introduction

Layered transition metal dichalcogenides (TMDCs) MX_2 (X = S, Se) have been among the first phases considered as host materials in intercalation reactions in which a guest species, atom, ion, or molecule, can be reversibly inserted into empty spaces of the host structure.[1−6] In the past the TMDCs have been extensively investigated because of the structural flexibility of the layered structures and their ability to adapt to the geometry of the inserted guest species by free adjustment of the interlayer separation. In compounds with neutral layers the interlayer bonding is of the van der Waals type and the interlayer space is a connected network of empty lattice sites. Hence, such crystals can be cleaved very easily, and the resulting surface is chemically saturated without dangling bonds.[7] One type of intercalation process may be described as a reversible topotactic reaction mediated by cation-electron transfer.[8] The interest in the intercalation process increased considerably after 1960 and has included other classes of layered materials such as, for

[†] University of Kiel.
[‡] Leibniz University Hannover.
[§] State University of New York at Stony Brook.
[||] LMU-Munich.

(1) Whittingham, M. S.; Jacobson, A. J. *Intercalation Chemistry*; Academic Press: New York, 1982.
(2) Rouxel, J. *Intercalated Layered materials*; D. Reidel: Dordrecht, The Netherlands, 1979; p 201.
(3) Dresselhaus, M. S. *Intercalation in Layered Materials*; Plenum Press: New York, 1986.
(4) Legrand, A. P.; Flandrois, S. *Chemical Physics of Intercalation*; Plenum Press: New York, 1986.
(5) Friend, R. H.; Yoffe, A. D. *Adv. Phys.* **1987**, *36*, 2.
(6) Rouxel, J. *Physica* **1980**, *B99*, 3.
(7) Jaegermann, W. In *Surface Studies of Layered Materials in Relation to Energy Converting Interfaces*; Aruchamy, A., Ed.; Kluwer: Dordrecht, The Netherlands, 1992.
(8) Schöllhorn, R. *Angew. Chem., Int. Ed. Engl.* **1980**, *19*, 983.

10.1021/ja076082+ CCC: $40.75

example, metal(IV) phosphates and phosphonates, transition metal oxyhalides, alkali-transition metal oxides, and especially clays like smectites, hectorites, and hydrotalcites.[9] The attention given to intercalated layered compounds can be attributed mainly to the fact that the host−guest interaction often changes significantly the chemical, catalytic, electronic, optical, and mechanical properties. Typical intercalation reactions occur near room temperature, and many intercalation compounds are metastable because of the inherent anisotropy in the chemical bonding. Thus, they are not easy to synthesize using other chemical routes like high temperature annealing. Soft chemical methods are powerful for the synthesis of such metastable phases. Intercalation reactions also provide routes for the synthesis of new solids with kinetic rather than thermodynamic stability.

In previous work on chemical intercalation with *n*-BuLi of the complex transition metal selenides Cr_4TiSe_8[10] and $Cr_3Ti_2Se_8$[11] we obtained several interesting and unusual results. The two compounds can host up to 2.8 and 2.7 Li per formula unit, respectively; i.e., the host material accepts nearly three electrons. One characteristic feature of the intercalation reaction was the irreversible phase transition of the starting material from monoclinic to trigonal symmetry. The structure of the resulting trigonal phases is very closely related to that of intercalated layered transition metal dichalcogenides, and the formulas $Li_xCrTi_{0.25}Se_2$ and $Li_xCr_{0.75}Ti_{0.5}Se_2$ for the two systems reflect this strong relationship. The monoclinic starting materials show a metal atom distribution with the Ti atoms preferring the fully occupied transition metal atom layers.[12,13] Li can be removed from the fully intercalated materials by treatment with water yielding finally $Li_{0.1}CrTi_{0.25}Se_2$ and $Li_{0.18}Cr_{0.75}Ti_{0.5}Se_2$. The different Li contents of the delithiated phases were explained on the basis of the differing electronic configurations of the two materials.[10,11]

Another interesting observation was made with ^{7}Li magic angle spinning (MAS) nuclear magnetic resonance (NMR) spectroscopy of the fully intercalated phases. At least two subspectra were observed for $Li_xCr_{1.25-y}Ti_ySe_2$ with $y = 0.25$, 0.5, 0.75, and 1.0, with isotropic NMR shifts in the range from +40 to −155 ppm. The large positive as well as negative shifts reflect the different environments of the Li ions, i.e., different types of paramagnetic cation neighbors. The magnetic properties of Cr_4TiSe_8[12] and $Cr_3Ti_2Se_8$/$Cr_2Ti_3Se_8$[13] were also studied, and their magnetic behavior is dictated by the metal atom distribution over the crystallographic sites and the electronic configuration. The disorder of Ti/Cr and competitive magnetic interactions leads to spin-glass properties at low temperatures. At higher temperatures the magnetic properties are dominated by low dimensional antiferromagnetic exchange interactions caused by very short Cr−Cr separations.[12] Introducing larger amounts of Ti changes the character of the *d* orbitals and consequently changes the magnetic properties of such compounds. It is well-known that the radial part of the *d* wave function of Ti extends more in space than that of Cr, thus favoring orbital overlap and the formation of extended bands. Our previous studies were devoted to the investigation of the reaction mechanism and the structural changes occurring upon Li intercalation. But obviously, the Li intercalation into a material like $Cr_2Ti_3Se_8$ should also significantly alter the physical properties such as the magnetic behavior. In this manuscript the changes of the structure and of the magnetic properties during lithium intercalation into $Cr_2Ti_3Se_8$ (or $Cr_{0.5}Ti_{0.75}Se_2$, using the notation used to describe the TMDC) are presented. ^{7}Li MAS NMR spectroscopy measurements are performed on the fully intercalated compound corresponding to $Li_{0.62}Cr_{0.5}Ti_{0.75}Se_2$ and compared with analogous measurements on the related compounds $Li_xCrTi_{0.25}Se_2$, $Li_xCr_{0.75}Ti_{0.5}Se_2$, and $Li_xCr_{0.25}TiSe_2$, corresponding to the fully intercalated compounds $Cr_{5-y'}Ti_{y'}Se_8$ with $y' = 1$, 2, and 4, respectively. Finally theoretical electronic structure investigations on the intercalated phases $Li_xCr_{0.5}Ti_{0.75}Se_2$ are discussed.

Experimental Section

Synthesis. The starting material $Cr_{0.5}Ti_{0.75}Se_2$ was prepared by high temperature solid-state reaction. A mixture of Cr (99.99%, Heraeus), Ti (99.5%, Chempur), and Se (99.99%, Retorte) in corresponding proportions was heated in evacuated sealed silica tubes to 950 °C at a rate of 100 °C/h and held at this temperature for 7 days, followed by subsequent cooling to room temperature over 6 h. The product consists of polycrystalline black platelets with a metallic luster. The phase purity was verified by X-ray diffraction and subsequent Rietveld refinements.

Chemical Analysis. The chemical composition of the samples was first determined with EDX analysis. Data were obtained using an accelerating voltage of 20 kV and a 60 s accumulating time. The presence of all three elements corresponding to the average composition of $Cr_{0.5}Ti_{0.75}Se_2$ ($Cr_{0.51(2)}Ti_{0.72(3)}Se_2$ with standard deviations estimated on the basis of the numbers of analyses). Finally, this composition was confirmed by means of Inductively Coupled Plasma (ICP) and Atomic Absorption Spectroscopy (AAS) analysis. The Li content of intercalated samples was determined with AAS.

Chemical Intercalation/Deintercalation. Chemical lithium intercalation was performed by immersing powdered samples of $Cr_{0.5}Ti_{0.75}Se_2$ in solutions of *n*-BuLi in hexane.[14] Hexane was dried with sodium and distilled before usage. To minimize the effect of crystallite size onto the time dependence of the intercalation reaction, powdered $Cr_{0.5}Ti_{0.75}Se_2$ was sieved prior to the reaction and only a well-defined fraction was used for intercalation. The average crystallite size of 10 to 50 μm was estimated from SEM micrographs. Typical experimental conditions were as follows: 0.5 g of $Cr_{0.5}Ti_{0.75}Se_2$ was mixed with 30 mL of hexane/20 mL of *n*-BuLi and transferred into test tubes which were then sealed. The tubes were kept under a dry argon atmosphere during the intercalation reaction which was done for 21 d at room temperature. Every day, a fraction of the reaction mixture was collected and washed three times with *n*-hexane in order to remove the surface lithium. These samples were then immediately characterized with X-ray diffraction and AAS analysis. The powder pattern of the material obtained after 7 d of intercalation showed the coexistence of two phases, i.e., reflections of the intercalated trigonal compound and of the pristine monoclinic material. The AAS analysis yields a Li content of 0.4, suggesting that the product is a mixture of $Cr_{0.5}Ti_{0.75}Se_2$ and $Li_{\approx 0.4}Cr_{0.5}Ti_{0.75}Se_2$ (Figure 1). This assumption is supported by the results of our earlier investigations which demonstrated that a small Li uptake by the monoclinic host leads to the formation of the new trigonal phase.[10,11]

(9) Alberti, G.; Costantino, U. *Solid State Supramolecular Chemistry*: *Two and Three-Dimensional Inorganic Networks*; Pergamon: New York, 1996; Vol. 7, Chapter 1, pp 1−23. Breu, J.; Stoll, A.; Lange, K. G.; Probst, T. *Phys. Chem. Chem. Phys*. **2001**, *3*, 1232. Breu, J.; Seidl, W.; Stoll, A.; Lange, K. G.; Probst, T. *Chem. Mater*. **2001**, *13*, 4213.
(10) Behrens, M.; Riemenschneider, O.; Bensch, W.; Indris, S.; Wilkening, M.; Heitjans, P. *Chem. Mater*. **2006**, *18*, 1569.
(11) Wontcheu, J.; Behrens, M.; Bensch, W.; Indris, S.; Wilkening, M.; Heitjans, P. *Solid State Ionics* **2007**, *178*, 759.
(12) Bensch, W.; Sander, B.; Näther, C.; Kremer, R. K.; Ritter, C. *Solid State Sci*. **2001**, *3*, 559.
(13) Wontcheu, J.; Kockelmann, W.; Huang, Zh.-Le; Bensch, W. *Solid State Sci*. **2007**, *9*, 506.
(14) Thackeray, M. M.; David, W. I. F.; Goodenough, J. B. *Mater. Res. Bull*. **1982**, *17*, 785.

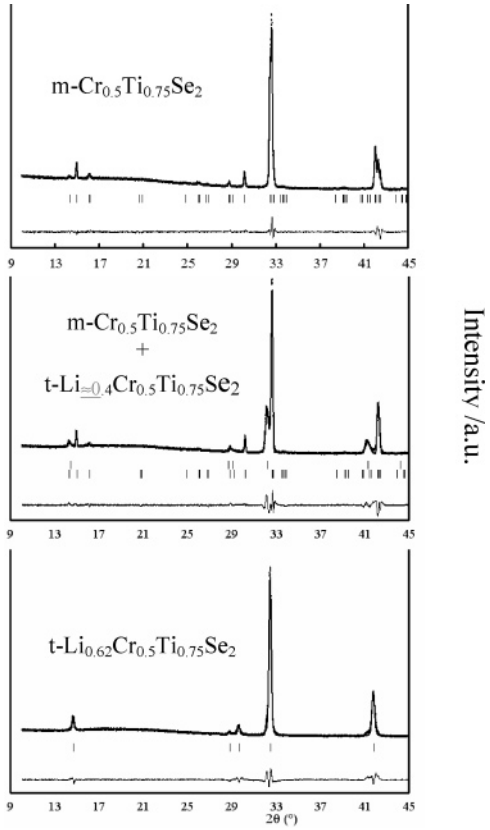

Figure 1. Rietveld refinement plots for $Cr_{0.5}Ti_{0.75}Se_2$ (top), $Cr_{0.5}Ti_{0.75}Se_2$/$Li_{\approx 0.4}Cr_{0.5}Ti_{0.75}Se_2$ (middle), and $Li_{0.62}Cr_{0.5}Ti_{0.75}Se_2$ (bottom). Observed intensities, circles; calculated intensities, continuous line; vertical bars, angular positions of the Bragg reflections. At the bottom, the difference $I_{obs} - I_{calc}$ is shown (only a selected region is outlined).

Li intercalation was also carried out at an elevated temperature (80 °C) for 4 days in a Teflon lined steel autoclave sealed under an argon atmosphere. The Li content of the material obtained with this method was much higher ($Li_{0.62}Cr_{0.5}Ti_{0.75}Se_2$), and only a single trigonal phase was observed in the powder pattern (Figure 1). The reversibility of the intercalation reaction was proven by reaction of the intercalated materials with distilled water at room temperature. For all reactions the final composition of the deintercalated samples was near $Li_{0.15}Cr_{0.5}Ti_{0.75}Se_2$ after 4 d of water treatment. After the deintercalation reaction was stopped after 1 d, a sample with composition $Li_{0.40}Cr_{0.5}Ti_{0.75}Se_2$ is obtained. In the powder pattern of this partially deintercalated phase only reflections of the trigonal material are present.

X-ray Diffraction (XRD) and Rietveld Refinement. X-ray powder diffraction patterns were recorded in transmission mode on a STOE Stadi-P diffractometer equipped with a position sensitive detector (PSD) and Ge monochromator using Cu Kα radiation ($\lambda = 1.540\,56$ Å). The angular range of 2θ was 10° to 90° with a 2θ step size of 0.01° and a counting time of 120 s for each step. The structure refinement was carried out by the Rietveld analysis[15−18] using the program Fullprof.[19] The background of the experimental data was interpolated linearly between selected points. The reflections were modeled with a pseudo-Voigt function. Preferred orientation was treated using March's approach. The atomic coordinates were refined without constraints, whereas the displacement parameter B_{iso} for Cr/Ti and all Se atoms were tied together during the refinement. The starting values for the atomic positions were those of the Cr_5Se_8 structure, in space group $F2/m$.[20] No absorption correction has been used. The metal atom distribution in $Cr_{0.5}Ti_{0.75}Se_2$ was determined using neutron scattering experiments, and four different metal positions were detected as previously observed in $Cr_{0.75}Ti_{0.5}Se_2$[13] while for $CrTi_{0.25}Se_2$[12] only three unique metal atom sites are occupied. Two sites (M(2), M(3)) are in the fully occupied metal atom layers, and two further sites (M(1), M(4)) are located in the metal deficient layers. A mixture of Cr and Ti is found over all metal positions with larger Ti concentrations in the fully occupied metal layers, with a very small amount of Ti on M(4). The experimental data for the parent material $Cr_{0.5}Ti_{0.75}Se_2$, the fully intercalated compound $Li_{0.62}Cr_{0.5}Ti_{0.75}Se_2$, the compound after 1 d of deintercalation $Li_{0.4}Cr_{0.5}Ti_{0.75}Se_2$, and the fully deintercalated phase $Li_{0.15}Cr_{0.5}Ti_{0.75}Se_2$ are summarized in Table 1. Note that standard deviations of the refined parameters have been multiplied by the Bérar−Lelann factor.[21] Powder diffraction patterns used for Rietveld refinement were taken immediately after intercalation. A structural diagram showing the arrangement of the metal sites in the structure of the monoclinic material and in the trigonal intercalated phase is presented in Figure 2 a and b.

^{7}Li Solid-State NMR. Room temperature ^{7}Li MAS NMR measurements were performed by using a Chemagnetics CMX 200 MHz spectrometer in combination with an Oxford 4.7 T cryomagnet at a Larmor frequency of 77.8 MHz. Spinning of the samples was performed in 1.8 mm rotors at 40 kHz. The temperature dependence of the spectra was studied on a Chemagnetics Infinity Plus 360 MHz spectrometer at 8.4 T corresponding to a Larmor frequency of 139.9 MHz. Spinning was performed in a 3.2 mm rotor at 17 kHz and at temperatures between 264 and 513 K. Temperature control was achieved by a gas flow of heated air or boil-off from liquid nitrogen for high and low temperatures, respectively. Calibration of the temperature measurement was performed via the ^{207}Pb resonance of solid $Pb(NO_3)_2$. This was particularly necessary at low temperatures since the spinning of the samples leads to additional heating. Due to this the temperatures could be measured with an accuracy of ±5 K. For the 2D NMR measurements, performed at 498 K, the spinning rate was reduced to 11 kHz. An aqueous solution of 1 M LiCl was used as an external reference for the NMR shifts in all cases. 1D NMR spectra were obtained with rotor-synchronized spin−echo experiments, and 2D NMR spectra were obtained via a common three-pulse 2D exchange sequence.[22,23]

Magnetic Susceptibility. The magnetic susceptibility of $Cr_{0.5}Ti_{0.75}Se_2$ as a function of temperature was measured using a Quantum Design MPMS XL SQUID magnetometer in a temperature range from 1.8 to 400 K at an applied field of 1 T. Both field-cooled (FC) and zero field-cooled (ZFC) measurements were performed. Powders (~80 mg) were loaded into precalibrated (300 K, 10 kOe) open quartz tubes and transferred into the magnetometer. The core diamagnetism and Pauli paramagnetism corrections have been done using $TiSe_2$ as a standard (7.0×10^{-5} emu/mol).[24] The susceptibility of the intercalated phases was measured from 2 to 300 K on a Quantum Design PPMS Evercool Low-Loss Dewar magnetometer with an external field of 1 and 0.1 T for FC and ZFC measurements, respectively. Samples were loaded into gelatine capsules inside an argon filled glovebox and immediately transferred to the magnetometer in order to avoid reaction of the materials with air and moisture. The phase pure trigonal samples $Li_{0.62}Cr_{0.5}Ti_{0.75}Se_2$ (fully intercalated), $Li_{0.40}Cr_{0.5}Ti_{0.75}Se_2$ (1 d of deintercalation) and $Li_{0.15}Cr_{0.5}Ti_{0.75}Se_2$ (4 d of deintercalation) were used for the magnetic measurements.

Band Structure Calculations. The present theoretical study of the magnetic properties of the compounds $Li_xCr_{0.5}Ti_{0.75}Se_2$ is based on

(15) Rietveld, H. M. *J. Appl. Crystallogr.* **1967**, *22*, 151.
(16) Rietveld, H. M. *J. Appl. Crystallogr.* **1969**, *2*, 65.
(17) Wiles, D. B.; Young, R. A. *J. Appl. Crystallogr.* **1981**, *14*, 149.
(18) Hill, R. J.; Howard, C. J. *J. Appl. Crystallogr.* **1985**, *18*, 173.
(19) Rodriguez-Carvajal, J. FULLPROF, XV Congress of International Union of Crystallography, Toulouse, 1990.
(20) Huppertz, H.; Lühmann, H.; Bensch, W. *Z. Naturforsch.* **2003**, *58b*, 934.
(21) Bérar, J.-F.; Lelann, P. *J. Appl. Crystallogr.* **1991**, *24*, 1.
(22) Duer, M. J. *Introduction to Solid-State NMR Spectroscopy*; Blackwell Publishing: Oxford, 2004.
(23) Levitt, M. H. *Spin Dynamics - Basics of Nuclear Magnetic Resonance*; Wiley: Chichester, 2004.
(24) Guy, D. R. P.; Friend, R. H.; Johnson, D. C.; Sienko, M. J. *Solid State Phys.* **1982**, *15*, 1251.

Table 1. Data of the Structure Refinements of $Cr_{0.5}Ti_{0.75}Se_2$, $Li_{0.62}Cr_{0.5}Ti_{0.75}Se_2$, $Li_{0.4}Cr_{0.5}Ti_{0.75}Se_2$, and $Li_{0.15}Cr_{0.5}Ti_{0.75}Se_2$

	$Cr_{0.5}Ti_{0.75}Se_2$	$Li_{0.62}Cr_{0.5}Ti_{0.75}Se_2$	$Li_{0.4}Cr_{0.5}Ti_{0.75}Se_2$	$Li_{0.15}Cr_{0.5}Ti_{0.75}Se_2$
crystal system	monoclinic	trigonal	trigonal	trigonal
space group	$F2/m$	$P\bar{3}m1$	$P\bar{3}m1$	$P\bar{3}m1$
a (Å)	12.380(3)	3.595(3)	3.592(3)	3.574(6)
b (Å)	7.151(2)			
c (Å)	11.834(3)	6.160(5)	6.094(2)	6.020(3)
β (deg)	90.196(1)			
V (Å^3)	1047.72(6)	68.96(1)	68.08(1)	66.62(2)
Z	4	1	1	1
2θ range (deg)	10−90	10−90	10−90	10−90
χ^2	1.89	4.21	7.76	6.57
R_{Bragg}	4.88	9.69	7.32	6.79
R_F	8.07	7.21	8.51	7.34

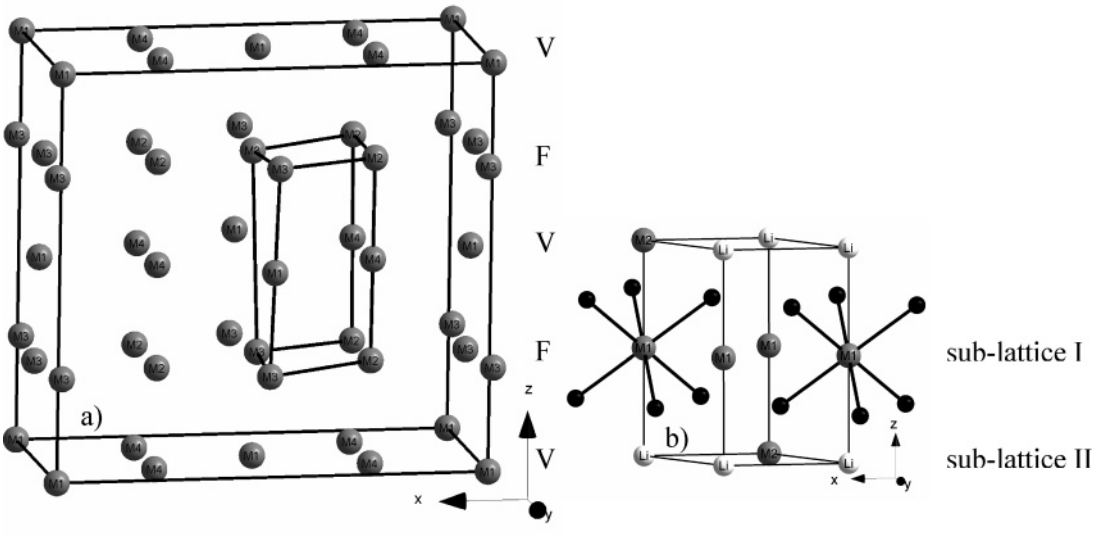

Figure 2. Crystal structure of (a) $Cr_{0.5}Ti_{0.75}Se_2$ (Se atoms are omitted for clarity; F denotes the fully occupied metal layer and V the partially occupied metal layer) and (b) $Li_{0.62}Cr_{0.5}Ti_{0.75}Se_2$ (Li atoms are shown just to get an insight on the possible Li sites in the unit cell).

electronic structure calculations which have been performed using the spin polarized relativistic Korringa−Kohn−Rostoker (SPR-KKR) band structure method in the atomic sphere approximation (ASA) mode.[25] Exchange and correlation were treated within the framework of the local spin density approximation (LSDA) of spin density functional theory, using the parametrization of Vosko, Wilk, and Nusair.[26] The chemical disorder in the studied materials has been described using the Coherent Potential Approximation (CPA).[27] The lattice parameters (e.g., a, c/a ratio) and atomic positions within the unit cell used in the calculations have been taken from the experiment.

Results and Discussion

The X-ray diffraction (XRD) patterns for the pristine material, the mixed phase obtained after 7 days of intercalation with *n*-BuLi, and the fully intercalated phase are shown in Figure 1. The powder pattern of $Cr_{0.5}Ti_{0.75}Se_2$ can be indexed in the nonconventional space group $F2/m$ of the monoclinic system. After about 7 days of intercalation, insertion of Li leads to the appearance of new reflections and the progressive disappearance of others. For instance, the (−402) reflection of $Cr_2Ti_3Se_8$ at 32.5° 2θ splits, and a new one appears which can be indexed as the (001) (32.29° 2θ) reflection of the trigonal system (space group $P\bar{3}m1$); on the low angle side of (−422), the (102) reflection of the trigonal material appears at 41.40° 2θ. In the powder pattern of the fully intercalated sample the three reflections of $Cr_{0.5}Ti_{0.75}Se_2$ between 14.30° and 16.06° 2θ have vanished and only the (001) reflection of the new phase is seen (14.44° 2θ). The lattice parameters of the new trigonal unit cell ($P\bar{3}m1$) are related to those of the pristine sample as follows: $a(Cr_{0.5}Ti_{0.75}Se_2) \approx 2\sqrt{3}a(Li_{0.4}Cr_{0.5}Ti_{0.75}Se_2)$, $b(Cr_{0.5}Ti_{0.75}Se_2) \approx 2a(Li_{0.4}Cr_{0.5}Ti_{0.75}Se_2)$ and $c(Cr_{0.5}Ti_{0.75}Se_2) \approx 2c(Li_{0.4}Cr_{0.5}Ti_{0.75}Se_2)$. The crystal structure of the newly developed trigonal phase is outlined in Figure 2 together with the structure of the monoclinic host material highlighting the close structural relationship between the two phases. For the sample obtained after 7 days of intercalation at room temperature both phases are present indicating inhomogeneously distributed Li. Probably, some regions of the crystallites are converted to the trigonal symmetry, whereas in others Li diffusion may be inhibited. It can also be imagined that some fraction of crystallites undergoes conversion more rapidly at intermediate Li contents. If the sample is stored in *n*-BuLi at room temperature for up to 21 d, no changes were observed in the powder pattern and the AAS analysis of such samples gives about 0.4 Li per formula unit. These observations are contrary to what has been observed for $CrTi_{0.25}Se_2$ and $Cr_{0.75}Ti_{0.5}Se_2$ upon intercalation applying the same method. The final compositions were $Li_{0.7}CrTi_{0.25}Se_2$ and

(25) Korringa, J. *Physica* **1947**, *13*, 392. Kohn, W.; Rostoker, N. *Phys. Rev.* **1954**, *94*, 1111. Ebert H. et al. The Munich SPR-KKR package, version 2.1.1, http://olymp.cup.uni-meunchen.de/ak/ebert/SPRKKR. Ebert, H. In *Electronic Structure and Physical Properties of Solids*; Dreyssé, H., Ed.; Springer: Berlin, 2000; p 191.
(26) Vosko, S. H.; Wilk, L.; Nusair, M. *Can. J. Phys.* **1980**, *58*, 1200.
(27) Soven, P. *Phys. Rev.* **1967**, *156*, 809. Stocks, G. M.; Temmerman, W.; Györffy, B. L. *Phys. Rev.* **1978**, *41*, 339.

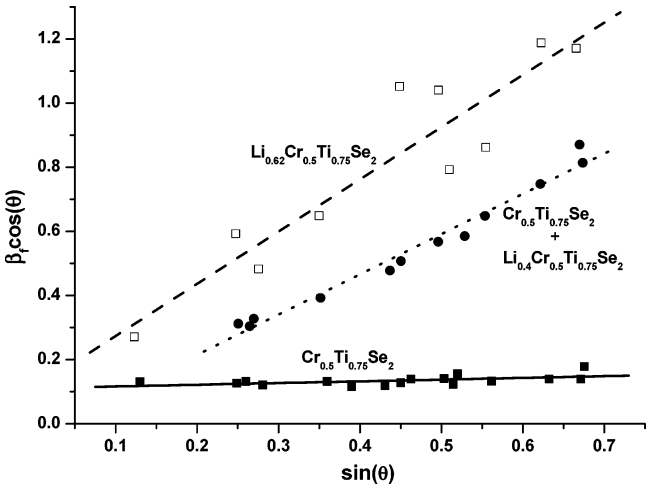

Figure 3. Williamson−Hall plot to identify the nature of line broadening after Li insertion into $Cr_{0.5}Ti_{0.75}Se_2$. (■) Reciprocal integral breadths β^* for selected, well resolved reflections of $Cr_{0.5}Ti_{0.75}Se_2$; solid line is the fit; (□) β^* for selected, well resolved reflections of $Li_{0.62}Cr_{0.5}Ti_{0.75}Se_2$; dashed line is the fit; (●) β^* for selected, well resolved reflections of $Cr_{0.5}Ti_{0.75}Se_2/Li_{\approx 0.4}Cr_{0.5}Ti_{0.75}Se_2$; dotted line is the fit.

$Li_{0.68}Cr_{0.75}Ti_{0.5}Se_2$ after about 21 d in *n*-BuLi.[10,11] In fact, in the $Cr_{5-y'}Ti_{y'}Se_8$ system the different metal atom substitutions alter the electronic structure and should change the resulting chemical behavior dramatically. From neutron scattering data[13] it is known that Ti atoms are mostly located in the full metal atom layers but their concentration on the partly occupied metal layers increases with y'. Due to the different Cr/Ti distribution, the energy for Li^+ ions to reach vacant sites between [$CrSe_6$] and [$TiSe_6$] octahedra is different for different y' values, and probably the energy of Li^+ is not large enough to reach vacant sites in $Cr_{0.5}Ti_{0.75}Se_2$ when the intercalation is performed at room temperature. In fact, one can assume that the kinetics is quite different depending on the nature of the cation in the partially occupied layers and due to the different spacing between the layers. The repulsive Coulomb interaction between the Li^+ ions which is expected to be responsible for the limitation of the lithium content[28,29] may be somewhat larger in $Cr_{0.5}Ti_{0.75}Se_2$ than in $CrTi_{0.25}Se_2$ and $Cr_{0.75}Ti_{0.5}Se_2$ at room temperature.

If the intercalation is carried out at 80 °C after 4 days the composition $Li_{0.62}Cr_{0.5}Ti_{0.75}Se_2$ is reached, and all the monoclinic material has been transformed to the trigonal Li intercalated phase (Figure 1). The Rietveld refinements showed a line broadening of the reflections of the fully intercalated phase, typically caused by domain size and/or strain effects. The broad peak width and weak diffraction intensity suggest that both the crystallinity is poor and the crystallite sizes are small for the intercalated samples. Using fwhm values leads to an overestimation of the crystallite sizes, and therefore a line profile analysis (LPA)[30] has been performed to get an impression as to what microstructural effects are responsible for the peak broadening. The Williamson−Hall plot[31] is displayed in Figure 3 for the pristine, the mixed phase $Cr_{0.5}Ti_{0.75}Se_2/Li_{\approx 0.4}Cr_{0.5}Ti_{0.75}Se_2$, and the fully intercalated material $Li_{0.62}Cr_{0.5}Ti_{0.75}Se_2$. The

Table 2. Compared M−M Contacts in the Pristine Material, 7 d Intercalation, Fully Intercalated, and Deintercalated Materials

	M1–M3 (Å) interlayer	M2–M4 (Å) interlayer	M2–M2 (Å) intralayer	M2–M3 (Å) intralayer
m-$Cr_{0.5}Ti_{0.75}Se_2$, pristine material	3.027(7)	2.959(5)	3.384(8)	3.460(9)
m-$Cr_{0.5}Ti_{0.75}Se_2$, after 7d intercalation	3.013(1)	2.954(2)	3.365(2)	3.412(4)

	M1–M2 (Å) interlayer	M1–M1 (Å) intralayer
t-$Li_{0.62}Cr_{0.5}Ti_{0.75}Se_2$, fully intercalated	3.080(2)	3.595(3)
t-$Li_{0.4}Cr_{0.75}Ti_{0.5}Se_2$, after 1d deintercalation	3.047(3)	3.592(3)
t-$Li_{0.15}Cr_{0.5}Ti_{0.75}Se_2$, after 4d deintercalation	3.010(2)	3.574(2)

data points of the fully intercalated material are approximately on a straight line with a positive slope, while for the pristine material the slope is significantly smaller. This indicates that pronounced strain occurs in the intercalated material and an estimation yields an enhancement of the strain by a factor of 6.6. In addition, the apparent size of diffracting domains is 620 Å for $Cr_{0.5}Ti_{0.75}Se_2$, whereas for $Li_{0.62}Cr_{0.5}Ti_{0.75}Se_2$ the value amounts to 120 Å indicating a decrease of the coherent diffraction domains upon intercalation. From Figure 3 it is also obvious that considerable strain was already developed in the material after 7 d of intercalation, which brings the intercalation process to an end. An increase of the temperature to 80 °C may reduce some strain, and further Li atoms can be inserted into the host material. The apparent size of diffracting domains was about 240 Å for this phase.

As previously observed for $CrTi_{0.25}Se_2$[10] and $Cr_{0.75}Ti_{0.5}Se_2$,[11] deintercalation is possible by treating the fully intercalated sample in distilled water for several days. The characteristic feature observed after this treatment is the contraction of the unit cell, but there are no hints of a switching back to the initial monoclinic phase; i.e., the transformation from monoclinic to trigonal symmetry is irreversible. After water treatment, the compositions were $Li_{0.4}Cr_{0.5}Ti_{0.75}Se_2$ (after 1 d) and $Li_{0.15}Cr_{0.5}Ti_{0.75}Se_2$ (after 4 d). The lattice parameters for the fully intercalated and deintercalated phases change as well as the M−M contacts (Tables 1 and 2). The contraction of the *c*-axis is much more pronounced than that of the *a*-axis. For intercalated TMDC materials, the variation of the *c*-axis has been attributed to both geometric and electronic effects,[32] and consequently the contraction observed for the *c*-axis of the pseudo-layered $Cr_{0.5}Ti_{0.75}Se_2$ upon Li deintercalation clearly demonstrates the structural relationship of the title compound with TMDC A_xMQ_2 (A = alkali metal, M = metal of groups 4 to 6, and Q = S, Se, Te) intercalation systems. The evolution of the M−Se distances with Li content reflects the influence of the change in the metal oxidation state. Mean values for different metal atom sites in both the monoclinic and trigonal phases are outlined in Table 3. Analyzing critically the M−Se bond lengths for the trigonal phases, it is clear that they increase from those observed following 7 days of intercalation to the fully intercalated state and decrease again upon Li removal. These findings demonstrate that the Li insertion into the host leads to a net

(28) Cava, R. J.; Murphy, D. W.; Zahurak, S.; Santoro, A.; Roth, R. S. *J. Solid State Chem.* **1984**, *53*, 64.
(29) Zachau-Christiansen B.; West, K.; Jacobsen, T.; Atlung, S. *Solid State Ionics* **1988**, *28−30*, 1176.
(30) Langford, J. I.; Louer, D.; Sonneveld, E. J.; Visser, J. W. *Powder Diffract.* **1986**, *1*, 221.
(31) Williamson, G. K.; Hall, W. H. *Acta Metal.* **1954**, *1*, 22.
(32) Rouxel, J. *J. Chim. Phys. Phys.-Chem. Biol.* **1986**, *83*, 841−850.

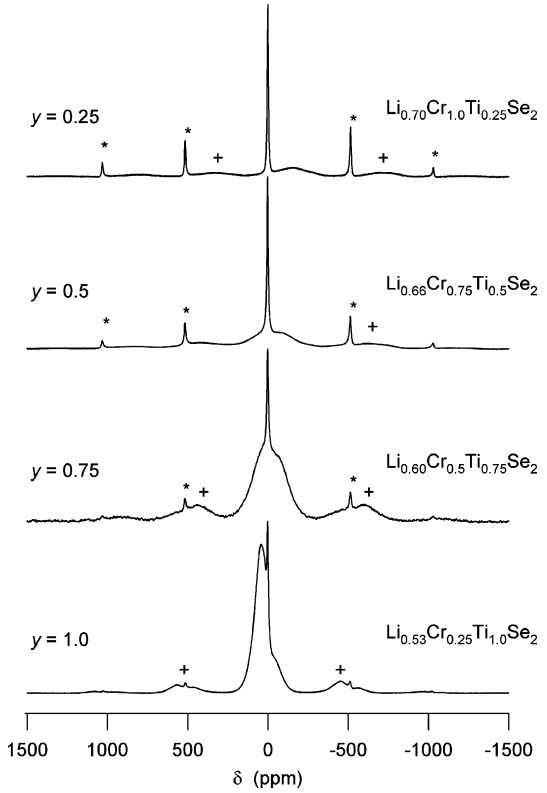

Figure 4. Room-temperature ^{7}Li MAS NMR spectra of $Li_xCr_{1.25-y}Ti_ySe_2$ for $y = 0.25$, 0.5, 0.75, and 1.0. Spectra were taken at a spinning speed of 40 kHz. Spinning sidebands are marked with * and +.

Table 3. Compared M−Se Distances in the Pristine Material, 7 d Intercalation, Fully Intercalated, and Deintercalated Materials

	M1–Se	M2–Se	M3–Se	M4–Se
m-$Cr_{0.5}Ti_{0.75}Se_2$, pristine material	2.534(8)	2.550(10)	2.571(3)	2.517(7)
m-$Cr_{0.5}Ti_{0.75}Se_2$, after 7d intercalation	2.530(8)	2.549(2)	2.555(3)	2.538(8)
t-$Li_{0.4}Cr_{0.5}Ti_{0.75}Se_2$, after 1d deintercalation	2.610(4)	2.546(4)		
t-$Li_{0.62}Cr_{0.5}Ti_{0.75}Se_2$, fully intercalated	2.618(2)	2.552(2)		
t-$Li_{0.15}Cr_{0.5}Ti_{0.75}Se_2$, after 4d deintercalation	2.584(1)	2.526(1)		

decrease of the oxidation state of the metal atoms, which increases again after reoxidation due to the Li deintercalation. The comparison of the M−M and M−Se distances for the pristine monoclinic material and of the monoclinic phase present in the phase mixture after 7 d of intercalation at room temperature (Tables 2 and 3) are slightly different. The small decrease may be caused by an electron transfer from Li to the host material reducing the oxidation state of the metal centers. A similar observation was previously made during the intercalation of $Cr_3Ti_2Se_8$.[11]

The local structure around the Li ions and their dynamics at temperatures in the range between 264 and 513 K were studied via ^{7}Li MAS NMR measurements. Figure 4 shows the room-temperature spectra of the series $Li_xCr_{1.25-y}Ti_ySe_2$ for $y = 0.25$, 0.5, 0.75, and 1.0. The samples contain similar Li contents x of 0.70, 0.66, 0.60, and 0.53, respectively. All spectra show a narrow isotropic resonance at about 0 ppm. In addition, much broader resonances are present with larger shifts than typically observed for diamagnetic materials. These shifts are ascribed to the Fermi-contact interaction of the Li nuclear spins with spin density associated with the transition metal atoms.[33,34] Comparison with earlier measurements,[10,11] which were partly performed on samples from different batches, reveals that a very high spinning speed in combination with a low magnetic field is essential for all spectral features to become apparent and to be assigned correctly.[35]

For the sample with $y = 0.25$, a broad resonance is present with a maximum at about −155 ppm, in addition to the narrow peak at 0 ppm. The broad resonance occurs at about −70 ppm for the sample with $y = 0.5$. The sample with $y = 0.75$, which is the main focus of this paper, shows a broad, asymmetric feature at around 0 ppm, which indicates that resonances are present with positive as well as negative shifts. In the case of $y = 1.0$ a clearly resolved, broad resonance is visible at about +40 ppm. It has a shoulder which again reveals the presence of local environments which give rise to negative shifts. Overall, with increasing Ti-content y, the broad features in the spectra shift to more positive shifts, and they become narrower. Furthermore, the spinning sideband manifold of the peak at 0 ppm becomes narrower with increasing y. This reflects the fact that the paramagnetism in these samples is reduced with decreasing Cr content. The negative shifts for the Cr-rich samples are caused by the presence of Cr^{3+} ions, which result in the transfer of spin density to the Li ions via the Se atoms, via Li−Se−Cr connectivities with bond angles of about 70° and 130°. These negative shifts are in agreement with ^{6}Li NMR results on Cr-doped $LiCoO_2$ and $LiMnO_2$ and on La_4LiCrO_8 where 90° Li−O−Cr bond angles result in small positive shifts while 180° bond angles give larger negative shifts.[33,36] The positive shifts that occur for the Ti-rich samples are ascribed to the increased concentrations of Ti^{2+} and Ti^{3+}.

Figure 5 shows the temperature dependence of the sample with $y = 0.75$, i.e., $Li_{0.62}Cr_{0.5}Ti_{0.75}Se_2$, for temperatures between 264 and 513 K. The maximum spinning speed was limited to 17 kHz due to the probe used in theses variable temperature studies, as compared to the room temperature measurement where a spinning speed of 40 kHz was possible. At low temperatures, the 0 ppm resonance is still clearly visible (labeled A) along with a broad feature, spreading over a range of about ±1000 ppm. Comparison with Figure 4 suggests that this broad feature is formed by broad overlapping spinning sidebands, which cannot be well resolved due to the slower spinning. At temperatures above 323 K the broad bump disappears and only the 0 ppm peak remains. When the temperature is increased further, a second peak (labeled B) appears above 448 K. It has a temperature-dependent shift, shifting from −39 ppm at 448 K to −21 ppm at 513 K. The temperature dependence suggests that peak B with its spinning sidebands corresponds to the broad low-temperature bump, which is now narrower at elevated temperatures. The disappearance of this resonance at intermediate temperatures reveals the onset of Li motion with correlation times τ_c [ms] shorter than about $(\omega_0\delta/\omega_r)$.[237] ω_0 is the Larmor frequency, ω_r is the rotation frequency, and δ is the line width in ppm. From this, one can obtain a rough estimate for τ_c of

(33) Carlier, D.; Menetrier, M.; Grey, C. P.; Delmas, C.; Ceder, G. *Phys. Rev.* **2003**, *B67*, 174103.
(34) Grey, C. P.; Dupré, N. *Chem. Rev.* **2004**, *104*, 4493.
(35) In Figure 10 of ref 10, the chemical shift axis was misaligned.
(36) Pan, C.; Lee, Y. J.; Ammundsen, B.; Grey, C. P. *Chem. Mater.* **2002**, *14*, 2289.
(37) Matti, Maricq, M.; Waugh, J. S. *J. Chem. Phys.* **1979**, *70*, 3300.

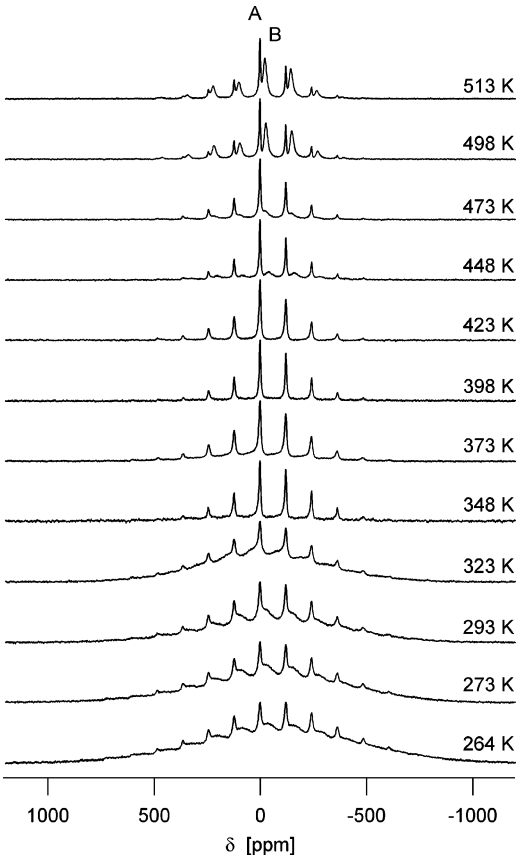

Figure 5. Temperature dependence of the ^{7}Li MAS NMR spectrum of $Li_{0.62}Cr_{0.5}Ti_{0.75}Se_2$. Spectra were taken at temperatures between 264 and 513 K and a spinning speed of 17 kHz.

<10 ms for temperatures above 340 K. At higher temperatures even faster motion causes an averaging of local fields around the Li nuclei and therefore a reappearance of the resonance with a narrower peak width. This occurs when the correlation time drops to below the inverse line width, and a rough estimate for the correlation time of $\tau_c < 10$ μs for temperatures above 440 K can be obtained. Peak A is not influenced by the motion associated with peak B. Several temperature runs with increasing and decreasing temperature were performed which revealed that the temperature variation of the spectra is completely reversible.

From the outset, it is not clear whether peak A and B stem from two different Li sites in the same compound or just from two different phases being present in the sample. To investigate this, a 2D NMR magnetization exchange experiment has been performed at 498 K, which is shown in Figure 6. The two peaks A and B are seen on the diagonal with NMR shifts of 0 ppm and −30 ppm, respectively, with their corresponding spinning sidebands. Only cross-peaks between the isotropic resonances and their spinning sidebands are seen and no cross-correlation peaks are visible that connect the different resonances, even at a mixing time of 50 ms, which suggests that the two resonances belong to two different phases. The peak shapes of peaks A and B are strikingly different. Whereas peak A has a Lorentzian shape, peak B shows a Gaussian line shape. This reveals that inhomogeneous broadening is present for peak B and furthermore suggests that motion of the Li ions between sites associated with different parts of the line shape leads to this Gaussian behavior.[38]

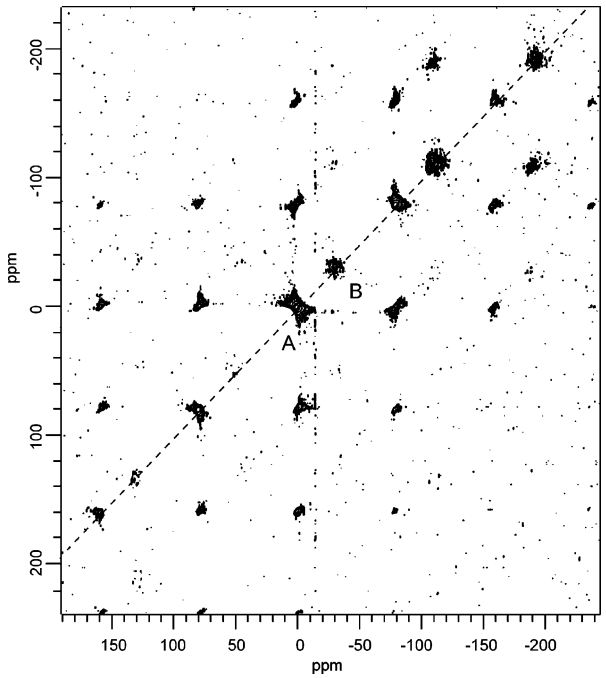

Figure 6. ^{7}Li 2D MAS NMR spectrum of $Li_{0.62}Cr_{0.5}Ti_{0.75}Se_2$ at 498 K and a spinning speed of 11 kHz. A mixing time of 50 ms was used.

1D NMR measurements performed with different recycle delays were analyzed, and a spin lattice relaxation time T_1 for the 0 ppm peak of about 0.4 s was extracted. For the peak at −30 ppm, $T_1 < 50$ ms. The large difference in the relaxation times for the two peaks confirms that the corresponding spin ensembles are well decoupled. The 0 ppm peak may therefore be ascribed to diamagnetic impurities formed during sample manipulation for the NMR experiments.

The temperature dependency of the magnetic susceptibility of the pristine material was determined in a previous study and is plotted in Figure 7a for comparison.[13] The experimental data were fitted using a modified Curie−Weiss equation $\chi = C/(T - \theta) + \chi_{tip}$, with a contribution due to temperature-independent paramagnetism (tip) $\chi_{tip} = 10^{-3}$ emu/mol. Although the magnitude of the magnetic susceptibility is large, it is similar to values that have been observed in previous studies of transition metal chalcogenide compounds.[39] The resulting magnetic parameters are outlined in Table 4. The large negative value for the Weiss constant θ of −113.5 K is indicative of strong antiferromagnetic exchange interactions between neighboring metal atoms that can be explained on the basis of the Goodenough and Kanamori rules.[40−43] The M−M separations within the fully occupied layers are 3.384(8) and 3.460(9) Å and the interlayer M−M contacts are 3.027(7) and 2.959(5) Å, indicating weak bonding interactions across the face sharing octahedra due to overlap of wave functions. Such direct exchange interactions are antiferromagnetic. Assuming that the Ti atoms are magnetically silent, an effective magnetic moment μ_{eff} of 3.91 μ_B per Cr atom can be calculated from the

(38) Ernst, R. R.; Bodenhausen, G.; Wokaun, A. *Principles of Nuclear Magnetic Resonance in One and Two Dimensions*; Oxford University Press: New York, 2004.
(39) Ohtani, T.; Sano, Y.; Kodama, K.; Onoue, S.; Nishihara, H. *Mater. Res. Bull.* **1993**, *28*, 501.
(40) Goodenough, J. B. *J. Phys. Chem. Solids* **1958**, *6*, 287.
(41) Goodenough, J. B. *Phys. Rev.* **1955**, *100*, 564.
(42) Kanamori, J. *J. Phys. Chem. Solids* **1959**, *10*, 87.
(43) Goodenough, J. B. *J. Phys. Chem. Solids* **1969**, *30*, 261.

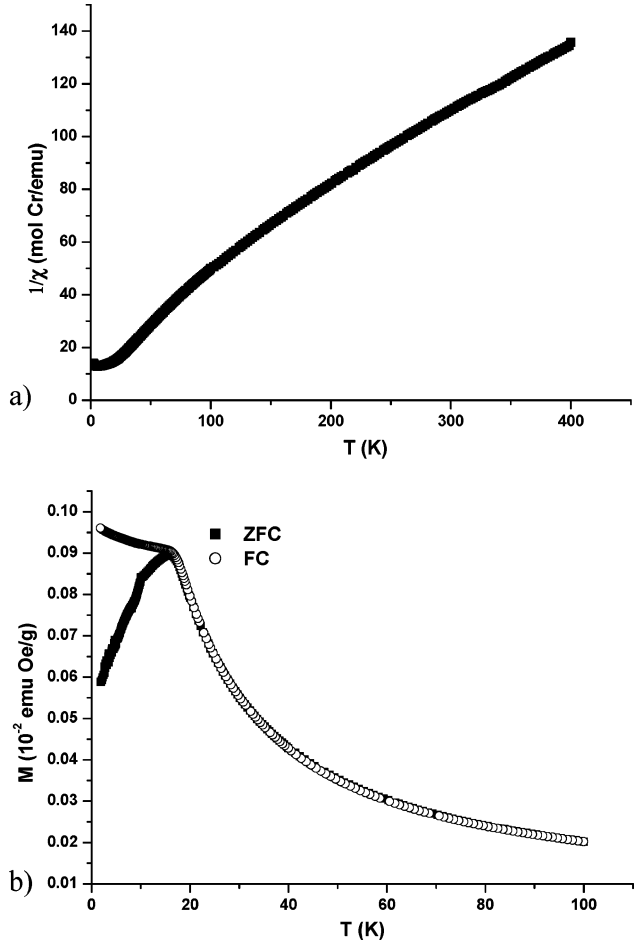

Figure 7. (a) Temperature dependency of the magnetic susceptibility at a field of 1 T for $Cr_{0.5}Ti_{0.75}Se_2$. (b) Temperature dependent M_{ZFC} and M_{FC} for $Cr_{0.5}Ti_{0.75}Se_2$.

Table 4. Magnetic Parameters for $Cr_{0.5}Ti_{0.75}Se_2$, $Li_{0.62}Cr_{0.5}Ti_{0.75}Se_2$ (Fully Intercalated), $Li_{0.4}Cr_{0.5}Ti_{0.75}Se_2$ (1 d Deintercalated) and $Li_{0.15}Cr_{0.5}Ti_{0.75}Se_2$ (4 d Deintercalated)

	μ_{eff} (μ_B/Cr)	θ_P (K)	T_{min}/T_{max} (K)	T_f (K)	T_c (K)
$Cr_{0.5}Ti_{0.75}Se_2$	3.91	−113.5	150/300	15.7	
t-$Li_{0.62}Cr_{0.5}Ti_{0.75}Se_2$	4.14	12	150/300	10	12
t-$Li_{0.4}Cr_{0.5}Ti_{0.75}Se_2$	3.86	7	150/300	7	8
t-$Li_{0.15}Cr_{0.5}Ti_{0.75}Se_2$	4.20	−28	150/300	6	6

experimental data, which is slightly larger than the theoretically expected value of 3.87 μ_B for d^3 but is similar to values often observed for chromium chalcogenides.[44] Shimada et al. explained this difference on the basis of an electron transfer from Se to Cr through *d*−p hybridization.[45] As can be seen in Figure 7b, above 20 K the ZFC and FC curves match perfectly but below that temperature the two curves deviate from each other. The splitting at 20 K indicates spin-glass behavior with the temperature where the two curves diverge determining the "freezing" temperature T_f.

Temperature-dependent magnetic susceptibilities were recorded for $Li_{0.62}Cr_{0.5}Ti_{0.75}Se_2$, $Li_{0.4}Cr_{0.5}Ti_{0.75}Se_2$, and $Li_{0.15}Cr_{0.5}Ti_{0.75}Se_2$, and the $1/\chi$ curves are shown in Figure 8a. Fitting the Curie−Weiss law to the linear regions yields $\mu_{eff} = 4.14$ μ_B, $\theta = 12$ K ($Li_{0.62}$); $\mu_{eff} = 3.86$ μ_B, $\theta = 7$ K ($Li_{0.4}$); and $\mu_{eff} = 4.20$ μ_B, $\theta = -28$ K ($Li_{0.15}$) (see Table 4).

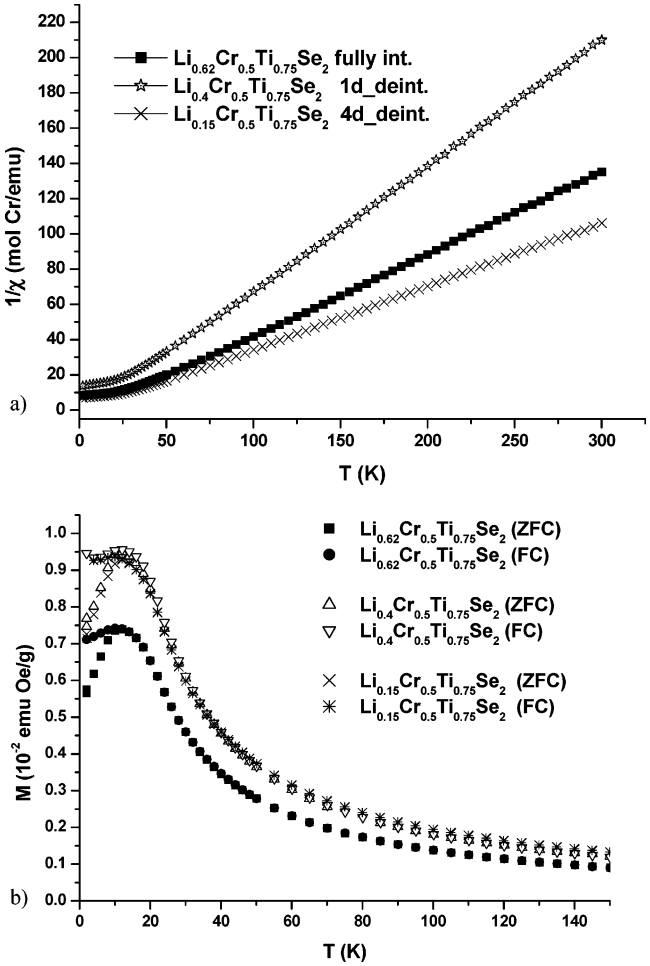

Figure 8. (a) Temperature dependency of the inverse magnetic susceptibility at a field of 1 T. (b) Temperature dependent M_{ZFC} and M_{FC} for $Li_{0.62}Cr_{0.5}Ti_{0.75}Se_2$, $Li_{0.40}Cr_{0.5}Ti_{0.75}Se_2$, and $Li_{0.15}Cr_{0.5}Ti_{0.75}Se_2$, respectively.

The most interesting observation is that the Weiss constant becomes more positive starting from −113.5 K for the pristine material and reaching 12 K for the fully intercalated sample. The simultaneous electron transfer during Li uptake alters the dominating magnetic exchange interactions, and obviously the ferromagnetic exchange becomes stronger with increasing Li content and the antiferromagnetic exchange is weakened. In the fully intercalated material the interlayer M−M separation between MSe_6 octahedra sharing common faces is 3.079(2) Å favoring antiferromagnetic interactions. But compared to the M−M distances of the host material this bond length is significantly larger; i.e., the strength of antiferromagnetic exchange interactions is smaller. The M−Se−M angles are nearly 90° in the trigonal samples mediating the superexchange more effectively than that in the monoclinic host compound. The intralayer M−M separation (Table 2) is too large for direct exchange interactions. In addition, if not all electrons are transferred into the conduction band but are localized on the different metal atoms the situation becomes more complex. In this case, a double exchange between, for instance, Cr(III) d^3 and Cr(II) d^4 must be invoked which is also ferromagnetic.

In order to answer the question of the magnetic ground states of the intercalated phases, the temperature dependence of ZFC and FC magnetizations was measured. The resulting magnetiza-

(44) Bensch, W.; Sander, B.; Helmer, O.; Näther, C.; Tuczek, F.; Shames, A. I.; Panich, A. M. *J. Solid State Chem.* **1999**, *145*, 235.
(45) Shimada, K.; Saitoh, T.; Namatame, H.; Fujimori, A.; Ishida, S.; Asano, S.; Anzai, S. *Phys. Rev.* **1996**, *53*, 7673.

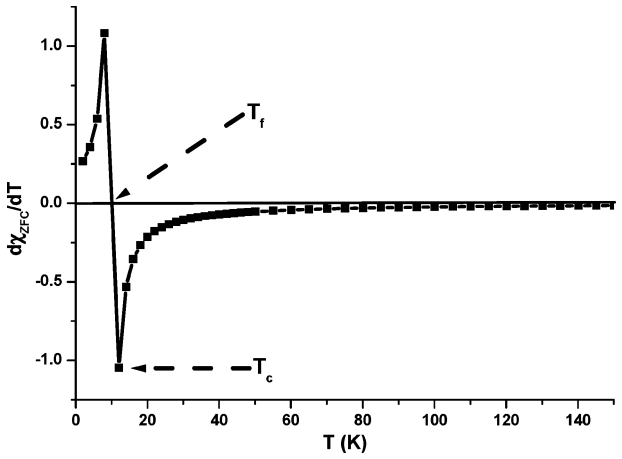

Figure 9. $[d_{\chi(ZCF)}/dT]$ as function of temperature for $Li_{0.62}Cr_{0.5}Ti_{0.75}Se_2$.

tion curves M_{ZFC} and M_{FC} are shown in Figure 8b. Here we define the freezing temperature T_f and a quasi Curie temperature T_c as follows (Figure 9, Table 4): T_f is the temperature at which $d_{\chi(ZCF)}/dT$ crosses the zero line while T_c is the temperature where the minimum of the $d_{\chi(ZCF)}/dT$ vs T curve occurs. In all cases the ZFC and FC curves superimpose at $T > T_f$ but deviate for $T < T_f$. These characteristics are typical of spin-glass behavior with the spins freezing into random orientations below T_f. We note that T_f decreases from 16 K for the pristine material to about 10 K for the fully intercalated phase with intermediate values for the other two intercalated samples (Table 4).

To complement the discussions of the magnetic properties of $Li_xCr_{0.5}Ti_{0.75}Se_2$ phases on the basis of the Goodenough−Kanamori−Anderson theory,[40−43] additional investigations were performed by ab initio electronic structure calculations. These calculations have been done with some approximations concerning the chemical order in the systems. Note that the TM (transition metal) sublattice is incompletely occupied and its occupation by the components (Cr, Ti, Li) is not clear from the experiment. The comparable problem of Cr distribution in $Cr_{1+x}(Te,Se)_2$ samples was discussed in detail in our previous work[46] where we found that the Cr sublattice consists of two sublattices which are completely (sublattice I) and incompletely (sublattice II) occupied. In the present calculations we used a similar approach to deal with the occupation of the TM sites. All Li atoms have been assumed to occupy the sites of the incomplete sublattice. However, there are also no clear experimental data concerning the distribution of Cr and Ti atoms in these two sublattices (I and II). Therefore, we considered two limiting configurations with all Ti atoms occupying the sites of the complete sublattice (configuration A) and with all Cr atoms distributed within the same complete sublattice (configuration B).

The calculations have been performed for the ferromagnetic state as a ground state of the system, instead of the spin-glass state observed in the experiment, with a subsequent analysis of electronic and magnetic properties. Comparing the dependence of the Cr magnetic moment on Li content, obtained in our calculations, with that observed in the experiment we should keep in mind the different meanings of these values. The experiment gives the so-called effective magnetic moment derived from the magnetic susceptibility obtained experimentally for the paramagnetic state, while the theoretical value of the Cr magnetic moment in the FM state corresponds to the saturation magnetization per Cr atom in the FM state of compounds and cannot be readily measured for the samples under consideration. Nevertheless, we assume that the reason for the modification upon increase of the Li concentration of these values obtained theoretically and in the experiment should be phenomenologically similar.

Figure 10a shows the values of the Cr spin magnetic moments obtained in our calculations for three compounds with Li concentrations $x = 0.15, 0.4, 0.62$, which have been investigated experimentally. The Cr spin magnetic moment corresponding to the configuration A increases monotonously with the Li concentration while for configuration B it is a nonmonotonous function of the Li content. Further calculations for configuration B were undertaken, i.e., for the samples with Li concentrations $x = 0, 0.25, 0.35, 0.45, 0.55, 0.75$, using the lattice parameters evaluated by interpolating the experimental values. As is seen in Figure 10a (dashed line), the Cr spin magnetic moment is about 3 μ_B for all materials with $x_{Li} < 0.35$ and $x_{Li} > 0.5$, while, in the middle region of the Li concentrations, the value drops to about 2.6 μ_B. This variation of the spin magnetic moment correlates with the variation of the electron charge densities (Figure 10b) connected to the sublattices I and II. The electron charge transfer between the sublattices I and II decrease when the Li concentration x_{Li} is within the region 0.35−0.5. We note that in the paramagnetic state of the system the charge distribution within the unit cell has a similar behavior upon variation of the Li content as it is found in the ferromagnetic state. This means that a variation of the Li content causes primarily a modification of the charge distributions in the compounds, which leads to corresponding nonmonotonous changes of the Cr magnetic moment obtained in our calculations. We assign this behavior of charge distribution in sublattices I and II to the competition between the potential and band (i.e., kinetic) energies of the electrons. Preferable conditions for a charge transfer deduced from the calculations seem to be connected with the occupation of the energy bands of the electrons, caused by the increase of the Li concentration. For example, the stability of the state with a small charge transfer between the sublattices I and II (as well as small magnetic moments) for $x_{Li} \approx 0.35-0.5$ is associated with a decrease of the band energy in this region of Li content (Figure 11).

The change of the charge distribution upon increase of the Li concentration is accompanied by modifications of the electronic density of states (DOS). In Figure 12a and 12b the DOS of *s*- and *p*-electrons corresponding to the sublattices I and II of the sample with $x_{Li} = 0.15$ are compared with the corresponding DOS for $x_{Li} = 0.4$. Since the DOS of the electrons with the opposite spin directions are very similar, Figure 12 presents only the DOS for the spin-up states. The DOS of *s*- and *p*-electrons in sublattice I increases essentially around −5 eV when the Li concentration x_{Li} changes from 0.15 to 0.4 and decreases simultaneously for the electrons in sublattice II, a behavior that correlates with the decrease of the charge excess in sublattice II and lack of charge in sublattice I. A pronounced modification of *d*-states of Ti upon variation of the Li content can be seen in Figure 12c. Both, in sublattice I and II the Ti DOS of *d*-states for the Li concentration $x_{Li} = 0.15$ is more

(46) Huang, Zh.-Le; Bensch, W.; Mankovsky, S.; Poleysa, S.; Ebert, H.; Kremer, R. K. *J. Solid State Chem.* **2006**, *179*, 2067. Wontcheu, J.; Bensch, W.; Mankovsky, S.; Poleysa, S.; Ebert, H. *J. Solid State Chem.*, submitted.

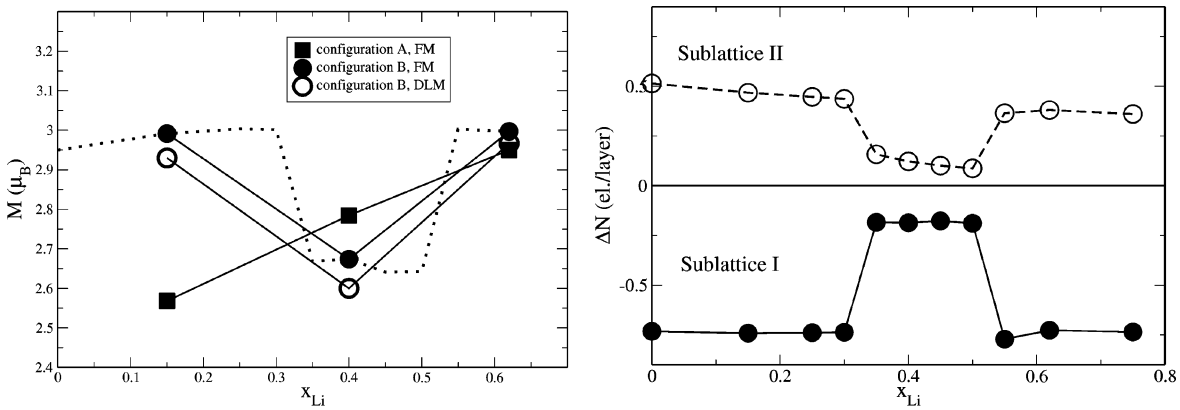

Figure 10. (a) Cr spin magnetic moments for configurations A and B in the FM state and those obtained within the DLM calculations for configuration B. Dashed line presents the results for configuration B in the FM state for intermediate Li concentrations; (b) the charge deviation from the neutral one in sublattices I and II obtained for configuration B.

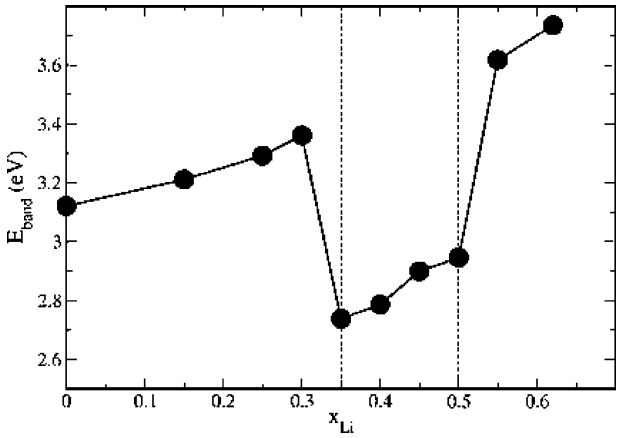

Figure 11. Variation of the electronic band energy upon variation of Li concentration for configuration B.

narrow than that for $x_{Li} = 0.4$. Essential changes of the DOS of *d*-electrons of Ti in sublattice II occur primarily for the nonoccupied states and do not influence remarkably the charge distribution in the samples. The DOS of the Cr *d*-states does not show essential changes upon variation of the Li concentration except for the decrease of the exchange splitting of spin-up and spin-down states for $x_{Li} = 0.4$, which results in the decrease of the Cr magnetic moment.

To model the high-temperature paramagnetic state, we performed calculations of the electronic structure within the Disordered-Local-Moment (DLM) model[47] which assumes a random distribution of spin magnetic moments. The Cr magnetic moments obtained in these calculations are close to the values obtained for the FM state and also exhibit a nonmonotonous dependence on the Li content, as is shown in Figure 10. On the basis of these results we assume that the modifications of the charge distribution caused in the system by variation of the Li content are responsible for the corresponding variation of the effective magnetic moment obtained experimentally for the high-temperature paramagnetic phase.

The DLM calculations show also that Cr magnetic moments are not sensitive to the alignment of the magnetic moments of the surrounding atoms. This means that the Heisenberg model can be a good approximation for the system under consideration to investigate its temperature-dependent magnetism using for example Monte Carlo simulations. In the present work, however, we make only an attempt to analyze the stability of the FM configuration within the Heisenberg model for the temperature regime for which a spin-glass ground state has been observed experimentally. The corresponding exchange coupling constants have been calculated using the expression given by Lichtenstein et al.[48] within the KKR Green's function formalism. Figure 13 shows the exchange coupling parameters calculated for the sample with $x_{Li} = 0.15$, for configurations A and B. In the second case the couplings with the first and second Cr neighbors (arranged in sublattice I) are negative. This indicates conditions for strain concerning magnetic order, as discussed in the literature, which can lead to noncollinear magnetic structures in the case of a completely occupied lattice but can create a spin-glass state in the present case with the half occupation of the sublattice I by Cr atoms.[49] These results are in line with the discussions presented above which are based on the rules derived within the Goodenough−Kanamori−Anderson theory.[40−43] The Cr1−Cr1, Cr1−Cr2, and Cr2−Cr2 exchange coupling parameters obtained for configuration A are also presented in Figure 13. In this case the exchange between Cr atoms corresponding to sublattices I and II are quite different. The distance dependence of Cr1−Cr1 exchange couplings within the fully occupied sublattice is similar to that obtained for configuration B. Such behavior of the interactions should lead to strain in the magnetic exchange that can be the reason for the appearance of a spin-glass state, similar to the situation for the configuration B. However, the coupling within sublattice II obviously should lead to the ferromagnetic ordering. Taking into account the exchange coupling between sublattices I and II, one can expect FM order in the material with configuration A, or at least a magnetic configuration with a nonvanishing total magnetic moment. Thus the results for the exchange coupling between Cr atoms for configuration B are in satisfying accordance with experiment. However, one should remember that we consider only two limiting cases of the Cr and Ti distribution (i.e.,

(47) Akai, H.; Dederichs, P.H. *Phys. Rev.* **1993**, *B 47*, 8739. Crisan, V.; Entel, P.; Ebert, H.; Akai, H.; Johnson, D. D.; Staunton, J. B. *Phys. Rev.* **2002**, *B66*, 014416.

(48) Lichtenstein, A. I.; Katsnelson, M. I.; Antropov, V. P.; Gubanov, V. A. *J. Magn. Magn. Mater.* **1987**, 67, 65.

(49) Bhatt, R. N.; Young, A. P. *PRL* **1985**, *54*, 924. Loison, D.; Schotte, K. D. *Eur. Phys. J.* **1998**, *5*, 735. Ruban, A. V.; Latsnelson, M. I.; Olovsson, W.; Simak, S. I.; Abrikosov, I. A. *PRB* **2005**, *71*, 054402.

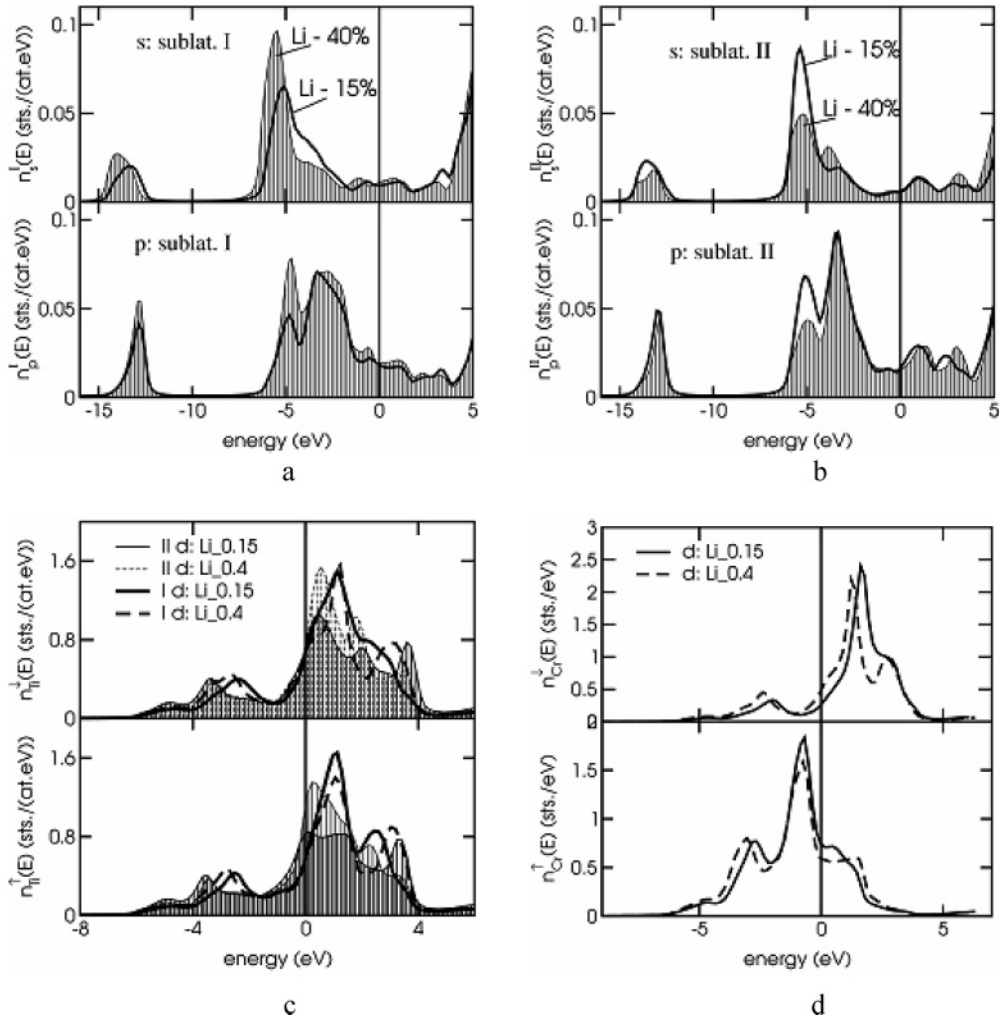

Figure 12. DOS of s- and p-spin-up electrons in sublattices I (a) and II (b); (c) DOS of Ti d-states in the two sublattices and (d) DOS of Cr d-states.

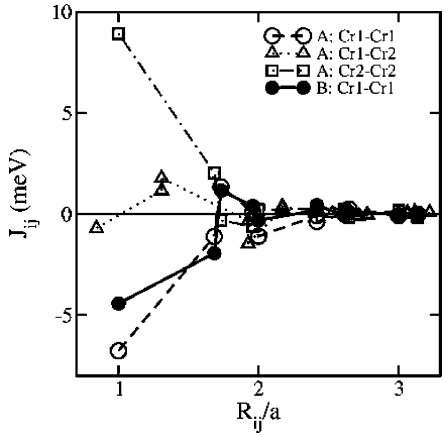

Figure 13. Comparison of the exchange coupling parameters between Cr magnetic moments calculated for configurations A and B of the sample having 15 at. % Li.

configurations A and B), while the real distribution can lie between these two limits.

In summary, our theoretical calculations show that the nonmonotonous behavior of the effective magnetic moment upon variation of Li concentration can be explained by corresponding changes in the electron charge distribution taking place in the completely and incompletely occupied TM sublattices. The exchange coupling parameters calculated for the FM state indicate the trend to create a strained magnetic structure. In the case of the compounds under consideration this implies the possibility for a spin-glass ground state as observed experimentally.

Conclusions

The Li intercalation into monoclinic $Cr_2Ti_3Se_8$ under mild reaction conditions leads to a phase transition forming a new trigonal phase with composition $Li_{0.62}Cr_{0.5}Ti_{0.75}Se_2$. The incorporation of Li^+ ions which is accompanied by an electron transfer from the guest ions to the host material significantly changes the bonding interactions and the electronic structures. The material can be deintercalated in a controlled way allowing a directional alteration of the structural and electronic properties. We note that the structural phase transition is not reversible which may be due to electronic reasons. The change of the geometric and electronic situation upon Li uptake leads to a drastic alteration of the magnetic properties of the material. Starting from strongly dominating antiferromagnetic exchange interactions in the pristine material, the magnetic behavior is tuned to dominating ferromagnetic exchange in the fully intercalated material. One should keep in mind that the tuning of the magnetic properties occurs under ambient conditions. To the best of our knowledge such a strong change of the magnetic behavior upon Li intercalation was never observed before in literature. The interesting alternating effective magnetic moment

per Cr atom as function of Li content can be explained on the basis of the electronic band structure calculations. Depending on the Li content the electron charge distribution is altered which is responsible for the change of the localized magnetic moment. The experimentally observed spin-glass behavior results from competing ferromagnetic and antiferromagnetic exchange interactions as well as from the disorder of the Cr/Ti atoms over the crystallographic sites. Obviously, the electronic structure calculations support the interpretation of our experimental findings. The Cr/Ti disorder is also confirmed by the ^{7}Li MAS NMR measurements that reveal a variety of transition metal environments around the Li sites. The NMR studies also exhibit fast Li dynamics with motional correlation rates between 10^2 and 10^5 s^{-1} for temperatures between 340 and 440 K.

Further studies on these materials with respect to the ionic and electronic conductivity as well as to electrochemical intercalation in Li batteries are under way.

Acknowledgment. We thank the State of Schleswig-Holstein and the Deutsche Forschungsgemeinschaft (DFG, SPP 1136) for the financial support of this work. We also thank Dipl.-Ing. Ulrike Westernströer (Institute of Geochemistry, University of Kiel) for chemical analysis (ICP) and Mrs. M. Rasmussen (Institute of Inorganic Chemistry, University of Kiel) for magnetic measurements. C.P.G. and S.I. thank the NSF via DMR0506120 for financial support.

JA076082+